Stress Wave Propagation Effects in Two- and Three-layered Composite Materials

A. TASDEMIRCI,[1] I. W. HALL[1,*] AND B. A. GAMA[2]
[1]*Department of Mechanical Engineering and*
[2]*Center for Composite Materials*
University of Delaware, Newark, DE 19716, USA

M. GUDEN
Department of Mechanical Engineering
Izmir Institute of Technology
Izmir, Gulbahce, Turkey

(Received March 4, 2003)
(Revised September 9, 2003)

ABSTRACT: Multilayer materials consisting of ceramic and glass/epoxy composites have been subjected to high strain rate compression testing using the Split Hopkinson Pressure Bar. The samples were extensively strain gaged so that dynamic data were generated directly from the samples during testing. Output data from the experiments were compared with numerical simulations of the same experiments and good agreement was noted. It was found that the stress distribution within samples was quite inhomogeneous and that stresses were highest in the region of the bar–sample interface. The presence of a rubber interlayer between the ceramic and glass/epoxy decreased the stress in both components but dramatically increased the degree of stress inhomogeneity.

KEY WORDS: multilayer structures, finite element analysis, mechanical properties, high strain rate.

INTRODUCTION

MECHANICAL TESTING OF conventional metallic materials at high strain rates is a relatively mature technical undertaking. Typical equipment includes the Split Hopkinson Pressure Bar (SHPB), flyer plate tests, and so forth. However, an increasing number of newer materials are being considered for applications where high strain rates are encountered and testing of these is more problematical. For example, many polymers

*Author to whom correspondence should be addressed. E-mail: hall@me.udel.edu

0021-9983/04/12 0995–15 $10.00/0 DOI: 10.1177/0021998304040564

require the use of viscoelastic bars in order to generate accurately measurable transmitted waves so the basic equations developed for data reduction using the SHPB cannot be applied directly [1]. Similarly, foam materials exhibit rapidly changing values of modulus, and shock waves can develop in these materials at quite low impact speeds (50–400 m/s) so again the simple data reduction procedures break down [2,3].

The present work was initially motivated by a need to understand the behavior of thick-section composite materials under dynamic loading conditions. Several authors have addressed the subject of impact of monolithic laminates of e.g., glass/epoxy and graphite/epoxy [4–14], as well as their penetration or perforation [14,15]. An elegant general method to address wave propagation in multilayered media has been presented by Nayfeh [16], but its application is limited here due to the internal damage generation and nonharmonic nature of the waves in the present work.

Major complications arise whenever two or more dissimilar materials are mounted in intimate contact and subjected to dynamic loading. Their differing moduli, and hence impedances, will cause complex wave reflection and transmission phenomena at each interface encountered. An example of such materials is provided by modern integral composite armor for vehicle applications as described by Gama et al. [17–19]. This type of material is required to provide ballistic protection at minimum weight and frequently contains several layers of different impedance, typically a ceramic layer followed by a thick composite plate of, e.g., glass fiber/epoxy. Mahfuz et al. [20] report a finite element method study of high velocity impact on such an integral armor material. Such approaches are necessary because full-scale trials of such assemblies are expensive and difficult to instrument and analyze and are, consequently, limited in number [10].

Development of such multilayer materials must be guided by synergistic modeling and experimental efforts since simple analytical descriptions such as 'conventional stress versus strain curves' are meaningless in these cases, particularly at high strain rate. The present work was undertaken, therefore, in order to contribute to the development of techniques to understand wave propagation effects in multilayer materials in general and to investigate how useful the SHPB, and possible experiments derivative from it, might be in providing experimental data to validate finite element models. With the experience gained from the present results, subsequent work will address higher strain rates and the shorter pulses typical of high velocity, short duration impact events.

EXPERIMENTS AND MODELING

Samples for this work were prepared from multilayered material plates in which the layers were of widely different impedances. The first samples consisted of two layers, namely, 13.96-mm thick alumina tiles bonded to a glass/epoxy backing plate. The *S*2 glass fiber woven fabric (24 oz/yd^2)/SC15 epoxy (toughened resin) composite plates of thickness 11.3 mm, were produced using the vacuum assisted resin transfer molding process. Later samples, consisting of three layers, were prepared by inserting a 2-mm thick layer of EPDM rubber between the ceramic and composite.

Cylindrical samples either 11.25 or 15.71 mm in diameter were core-drilled from the plates in the through-thickness direction. As part of the larger program, samples have been compression tested quasi-statically using a screw-driven Instron machine and at

various strain rates between 400 and 1200 s^{-1} using a Split Hopkinson Pressure Bar (SHPB) apparatus (the compression axis normal to fiber plane). However, the focus of the present report concerns a series of tests all of which were conducted on the SHPB apparatus with a striker bar velocity of ~16 m/s. It should be emphasized at this point that, although the elastic bars of the Hopkinson Bar apparatus has been used to generate the data used in the study, the tests themselves do not correspond to conventional SHPB tests.

The ceramic layer was always at the impacted side. The particular SHPB apparatus used consists of Inconel 718 bars, 356 mm long striker bar, 3450 mm incident and 1850 mm transmitter bars, all with a diameter of 19 mm. Further details of the experimental setup and standard data reduction routines are available elsewhere [21].

Samples were fitted with strain gages so as to monitor real-time strains (and stresses) during the course of the tests, most importantly the high strain rate tests where wave propagation effects were to be investigated. Strain gages with 0.79 mm element lengths were used generally, although several tests were also carried out with an array of gages designed to sample the strain simultaneously at several locations along the sample length and thus provide a strain/time/position map of the wave passage.

A three-dimensional SHPB finite element model has been used to study the stress wave propagation in these multilayer materials and also the individual components of it. Rubber is a highly nonlinear elastic material and the role of this nonlinear material has been studied by modeling the rubber layer with experimentally determined material data. The analyses were performed using a commercial explicit finite element code LS-DYNA 960. Two axes of symmetry were assumed so only one quarter of the bar was modeled. For each test modeled, the output was displayed at several locations within the sample as well as at the location of the strain gages on the incident and transmitter bars of the SHPB apparatus. The desired ideal result is, thus, that the output calculated from the model exactly matches the data measured by the strain gages on the sample as well as by the gages on the incident and transmitter bars since this would indicate that the model is accurately capturing the wave propagation behavior in the sample and bars.

The model has four components in contact; a striker bar of length 356 mm, an incident bar and a transmission bar each of length 1524.0 mm, and the specimen, the ceramic, rubber and composite thicknesses of which are 14.9, 1.52 and 10.6 mm, respectively. The bar diameter is 19.05 mm and the diameter of the specimen is 16.0 mm. The component materials are modeled with eight nodes solid elements and the interfaces are modeled with the automatic contact sliding interfaces without friction. The impact velocity of the striker bar ($V = 16.0$ m/s) has been defined as the initial condition and all other boundaries are traction free and can move in any direction. In order to save computation time, the simulation uses bars 1524 mm in length instead of full length bars. It will be seen later from the figures that this has the effect of decreasing the transit time between successive waves and shortening the wave duration slightly: however, it does not affect the basic wave-shapes or amplitudes. A few trial computations were carried out using full-length bars but, apart from the slightly smaller time window, no significant differences were found and the shorter bars were used.

Material properties used in the finite element code are shown in Table 1. The ceramic and composite have been modeled with an orthotropic elastic material. Rubber has been modeled with a two parameter, nonlinear material model based on the Mooney–Rivlin model for rubber. The Inconel bars have been modeled with an isotropic elastic material model.

Table 1. Material properties used in finite element models.

Material	Modulus of Elasticity (GPa)	Poisson's Ratio	Density (kg/m^3)	Other
Ceramic	370	0.22	3900	–
Rubber	–	0.495	1200	$A = 0.2$, $B = 0.8$ (MPa) Mooney–Rivlin Consts.
Composite	$E1 : 27.5$	$\nu_{21} : 0.108$	1850	$G_1 : 2.86$ (GPa)
	$E2 : 27.5$	$\nu_{31} : 0.18$		$G_2 : 2.14$ (GPa)
	$E3 : 11.8$	$\nu_{32} : 0.18$		$G_3 : 2.14$ (GPa)
Inconel	207	0.3	7850	

RESULTS

The present series of tests have been singled out for this particular study, first, in order to keep all experimental parameters constant as far as possible and, second, because at ~16 m/s samples underwent only limited damage but did not fail catastrophically. It was hoped, therefore, that all of the ceramic deformation and much of the composite deformation could be modeled as elastic deformation. The composite portions began to exhibit delamination and significant radial strain whereas the ceramic only exhibited occasional spalling from the edges of the impacted face. A more detailed fractographic study will be reported elsewhere.

Tests on Component Materials

Split Hopkinson Pressure Bar tests and simulations were first performed for the single material cases, i.e., ceramic only and composite only. Figure 1(a) and (b) show a comparison of the experimental and numerical simulation results for the ceramic sample and represent data from strain gages mounted on the incident and transmitter bars. Figure 2(a) and (b) present similar comparison data for a composite sample.

Clearly there is good consistency between the model and experiment. The principal difference between experimental and calculated data is a slightly lower resolution for the experimental data since the actual strain gages on the bars have a length of 3.2 mm and tend to average out, or 'smear', the data acquisition process whereas the calculation reports data from a specific element 1.6 mm in length on the sample surface. This observation should also be kept in mind for subsequent comparisons between experimental and calculated data from the bars.

Figure 3(a) shows the z-stress in a ceramic sample, calculated at three elements, one close to each interface and one at the specimen's midsection as indicated in the inset. It can be clearly seen that during the course of testing, the material experiences a nonuniform stress distribution, with the minimum occurring at the sample midlength. Figure 3(b) shows calculated data from similar elements on the composite sample and again a slightly inhomogeneous stress state is noted within the sample. It should be pointed out, however, that the position of the chosen elements is critical and the present elements were chosen approximately 2 mm from the ends of the samples in order to compare with data from strain gages: If, instead, the elements had been chosen within 0.2 mm of the specimen ends, the stresses would vary by a factor of almost 2 whereas Figure 3(a) and (b) show a variation of $< 10\%$. Figure 3(c) and (d) show the actual

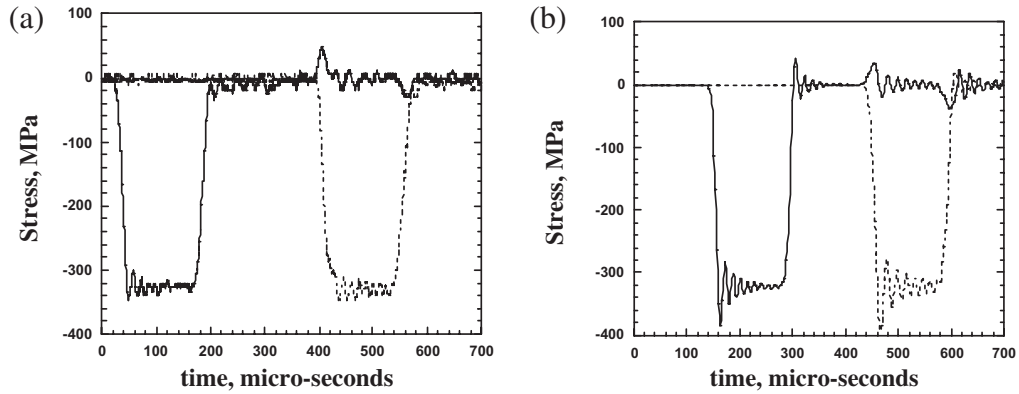

Figure 1. *(a) Experimental and (b) calculated output from strain gages on the incident and transmitter bars during a test on a ceramic sample.*

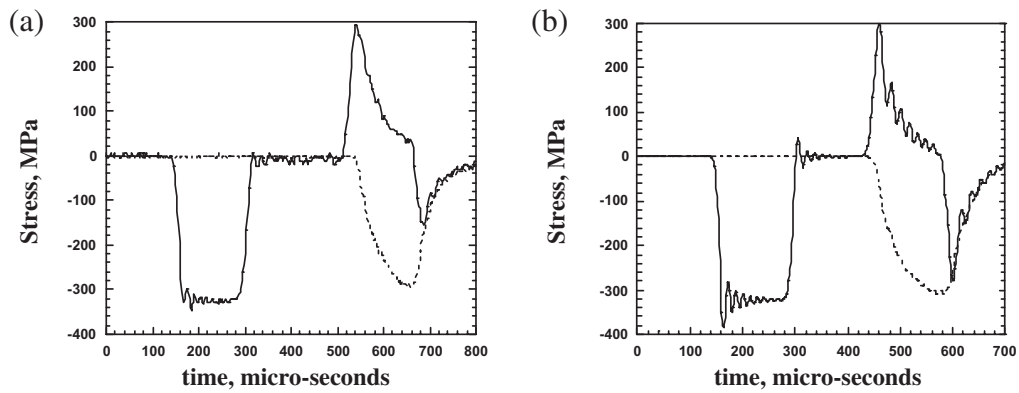

Figure 2. *(a) Experimental and (b) calculated output from strain gages on the incident and transmitter bars during a test on a composite sample.*

stress measured from a single strain gage at midlength of a sample for the ceramic and composite respectively. Again, the basic wave shapes and magnitudes are closely similar to the calculated values.

Figure 4 shows a comparison of data obtained from the same ceramic sample by all three routes, i.e., from conventional SHPB data reduction, from strain gage data and by LS-DYNA calculation from a midlength element. Some of the data have been time-shifted a little for clarity. Similar data for the composite samples show that the results are highly self-consistent for the single layer materials.

Tests on Two-layer Materials

Next, tests were performed on double layer, ceramic/composite samples and Figure 5(a) and (b) show experimental and calculated data from the Hopkinson bars. Again the data match closely, showing that LS-DYNA accurately captures the details of wave propagation. Note also, that the shape of the curves are not significantly different from

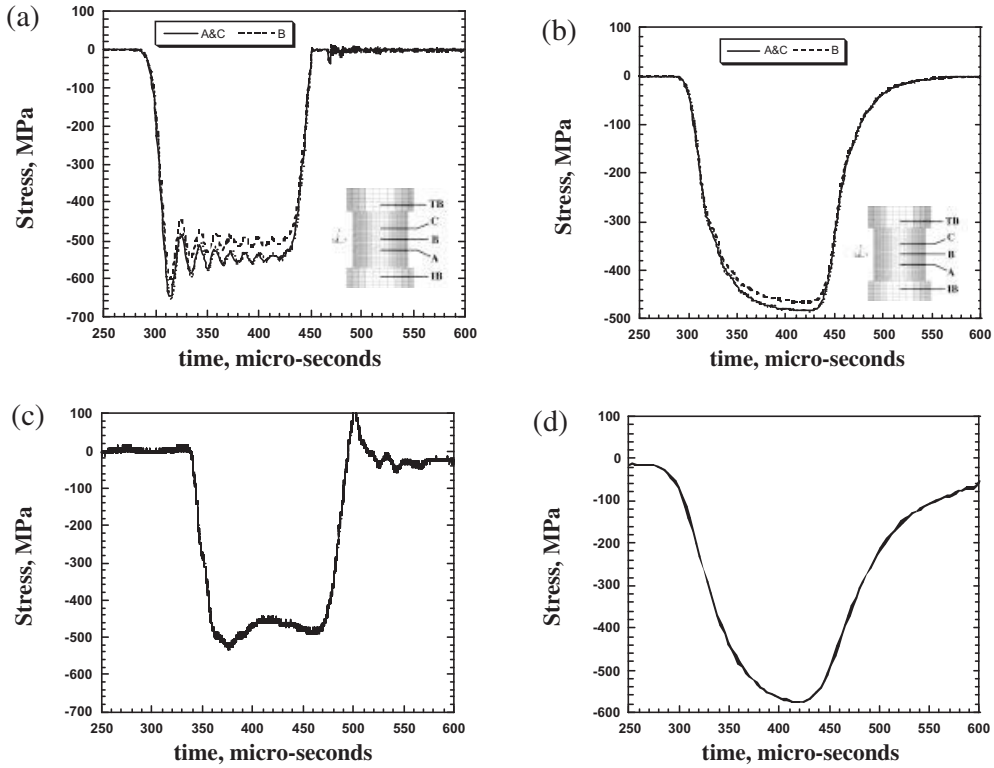

Figure 3. *(a) Z-stress calculated at three elements on a ceramic sample; (b) z-stress calculated at three elements on a composite sample; (c) measured z-stress at ceramic sample midlength during a test; (d) measured z-stress on composite sample midlength during a test.*

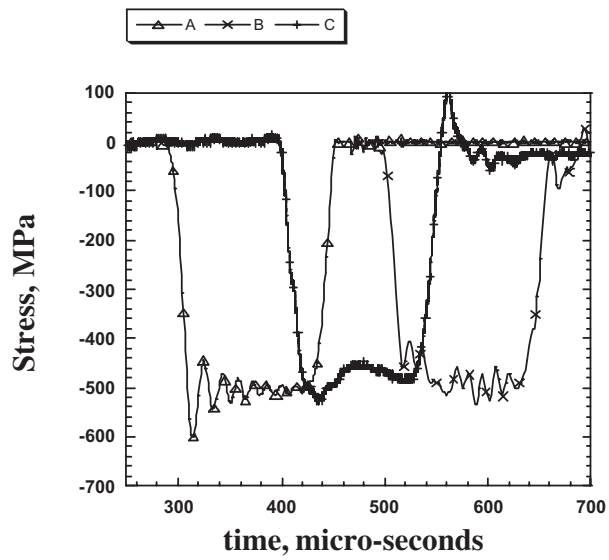

Figure 4. *Comparison of ceramic data obtained numerically (A), from strain gages (B), and by conventional SHPB data reduction routine, (C). (Data are time-shifted for clarity.)*

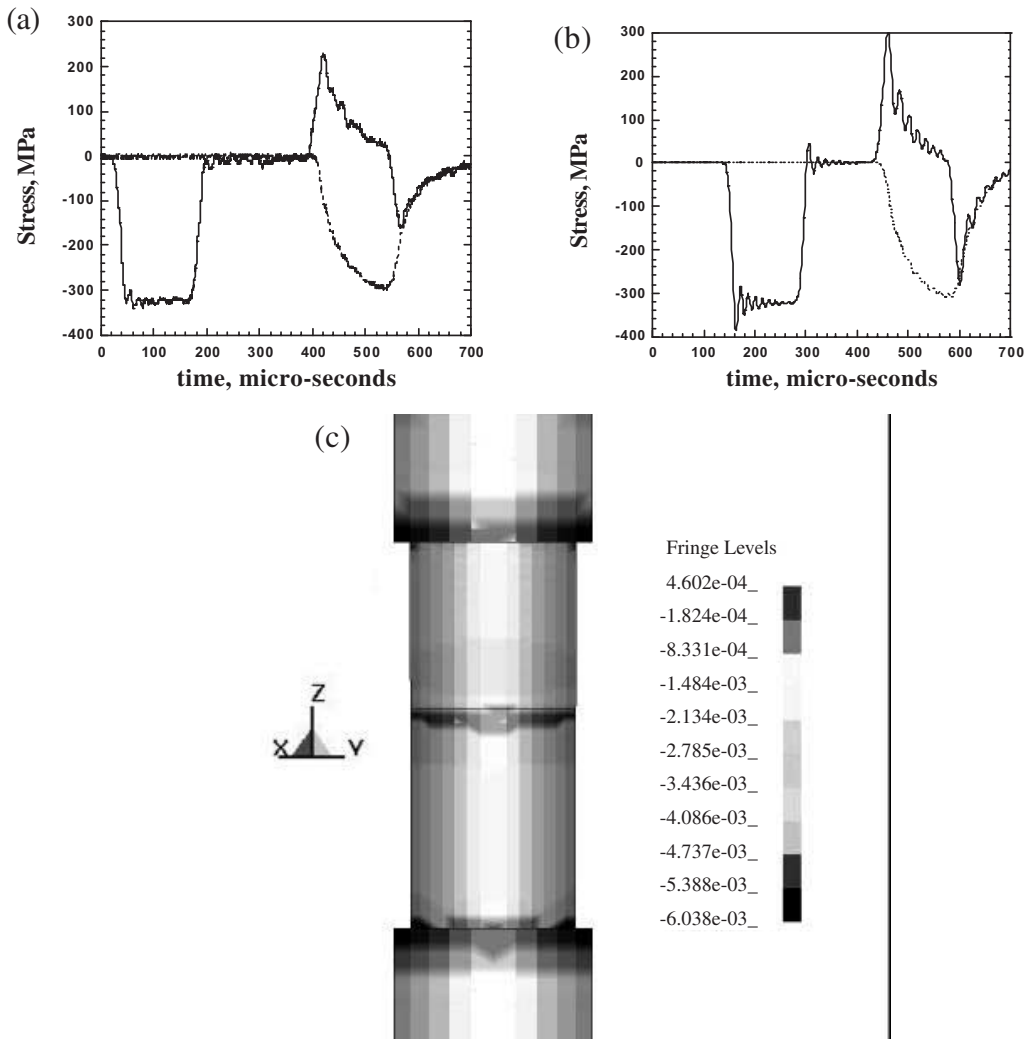

Figure 5. *(a) Experimental and (b) calculated output from strain gages on the incident and transmitter bars during a test on a two-layer, ceramic/composite, sample; (c) stress distribution within sample after 352 μs.*

the single layer composite cases, showing that the ceramic apparently has little effect on the response of the composite and essentially provides a hard loading block for the composite. Figure 5(c) shows the calculated stress distribution within the sample 352 μs after the start of the test.

Figure 6(a)–(d) show numerical and experimental data from the individual ceramic and composite layers respectively. The elements chosen for the numerical data were the same as for single layer tests in Figure 3(a) and (b) above and show a significantly greater amount of stress variation within the ceramic portion of the sample length. It is also noted that the shape of the z-stress response in the ceramic has changed from the single layer case and now closely resembles the response of the composite.

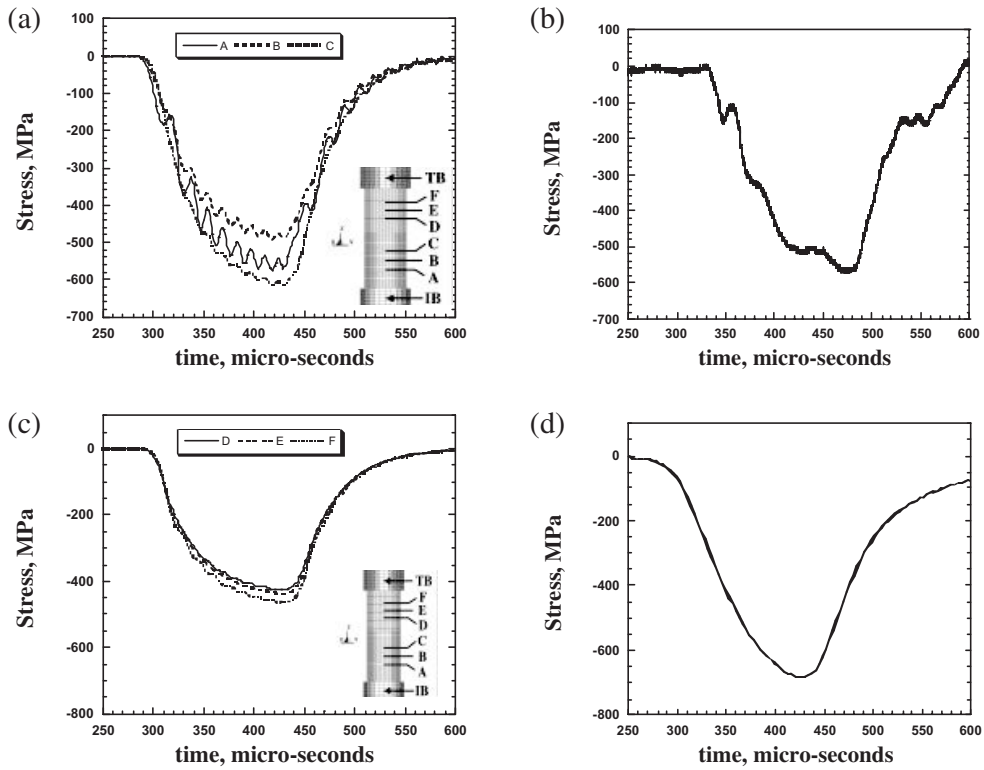

Figure 6. *Data from ceramic/composite sample: (a) calculated stress distribution at 3 elements within the ceramic; (b) measured stress from strain gage on ceramic midlength during a test; (c) calculated stress distribution at 3 elements within the composite, and, (d) measured stress from strain gage on composite midlength.*

Tests were also performed with the layer order reversed, i.e., the wave entered the composite first and then the ceramic. Experimental records from these composite/ceramic tests were essentially identical with those from ceramic/composite tests.

Tests on Three-layer Materials

A similar set of experiments and simulations was then carried out for the tri-layer material configuration, a configuration corresponding to one of the composite armor designs described in [19]. Now the presence of the rubber interlayer leads to major differences in the wave propagation characteristics. Data from the incident and transmitter bars, shown in Figure 7(a) and (b) show that a significantly greater fraction of the incident wave is reflected straight back to the incident bar with the consequence that a much reduced fraction enters the composite and, later, the transmitter bar. For these samples, agreement between the experimental and numerical data is currently slightly less close than for the single or two-layer cases for reasons which will be discussed further below. Figure 7(c) shows the stress distribution within the test sample 352 μs into the test.

Figure 8(a)–(d) show experimental and numerical data from the individual ceramic and composite layers respectively. The experimental data in Figure 8(a) were taken from gages

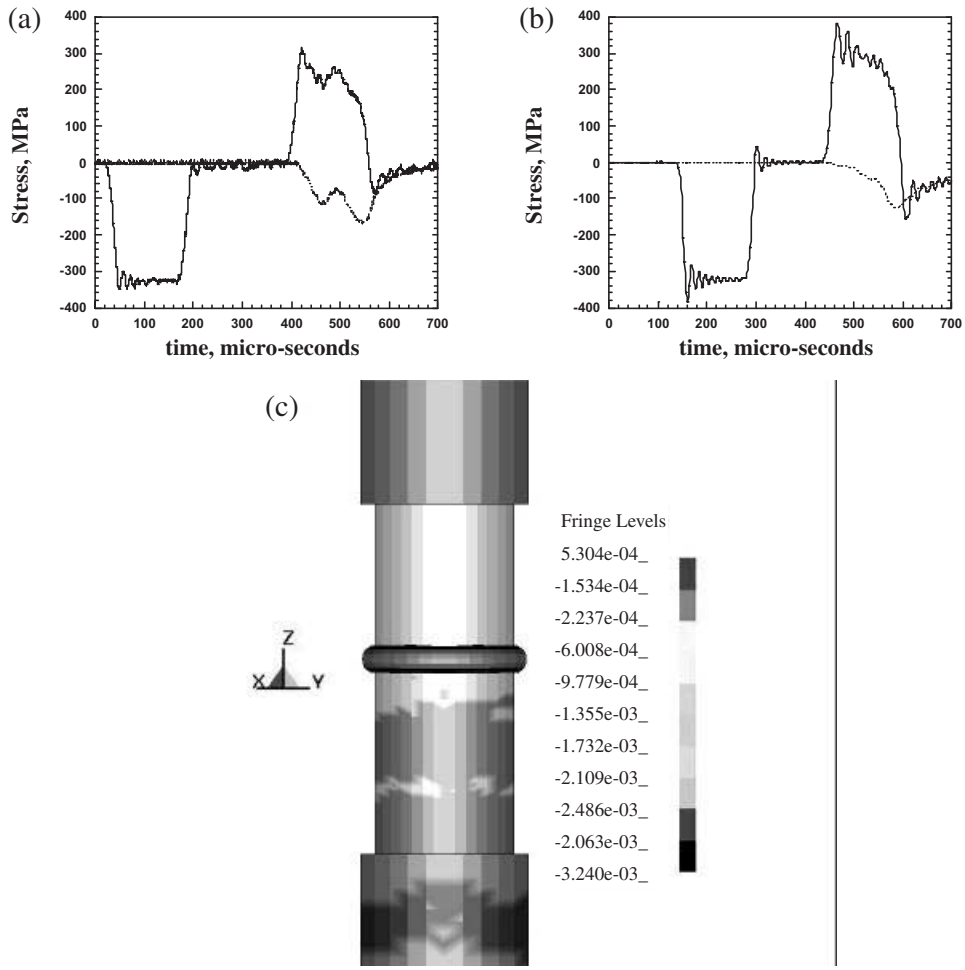

Figure 7. *(a) Experimental and (b) calculated output from strain gages on the incident and transmitter bars during a test on a tri-layer, ceramic/rubber/composite, sample: (c) stress distribution within sample after 352 μs.*

at two different locations, the first as close as possible to the incident bar–ceramic interface and the second close to the ceramic–rubber interface. Again, the elements chosen for the numerical data were the same as for single and double layer tests above but this time it is seen that there is a much greater amount of stress variation along the sample length. The measured and calculated z-stresses are consequently much more sensitive to the precise location of the data source. Thus, although the stress magnitudes differ in, e.g., Figure 8(c) and (d), the same general shapes are found, and the knee at $\sim 380\,\mu$s in the calculation is an indication of the first peak found experimentally. Also, note that the experimentally determined z-stress responses in ceramic and composite are now much more complex than in the single or double layer cases.

Figure 9(a) and (b) show a comparison, from the same elements, of the calculated z-stress results in the ceramic layer and composite layer for both the ceramic/composite and ceramic/rubber/composite configurations. The presence of the rubber very clearly

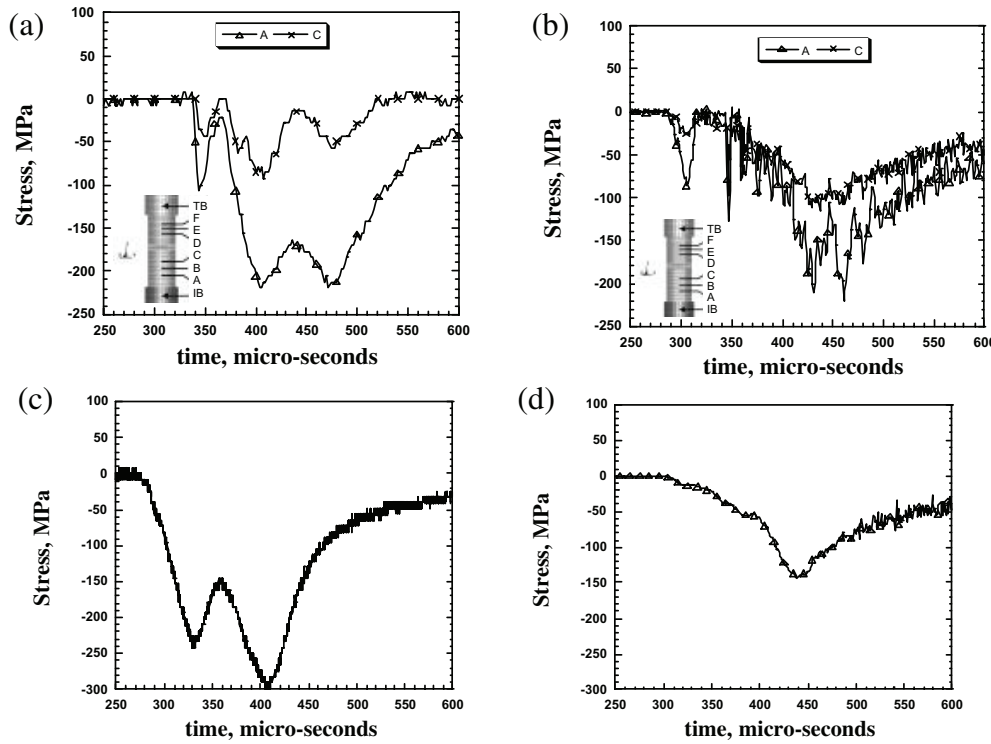

Figure 8. *Data from ceramic/rubber/composite sample: (a) measured stress from strain gage on ceramic; (b) calculated stress distribution at 2 elements within the ceramic; (c) measured stress from strain gage on composite; and, (d) calculated stress distribution at a midlength element within the composite.*

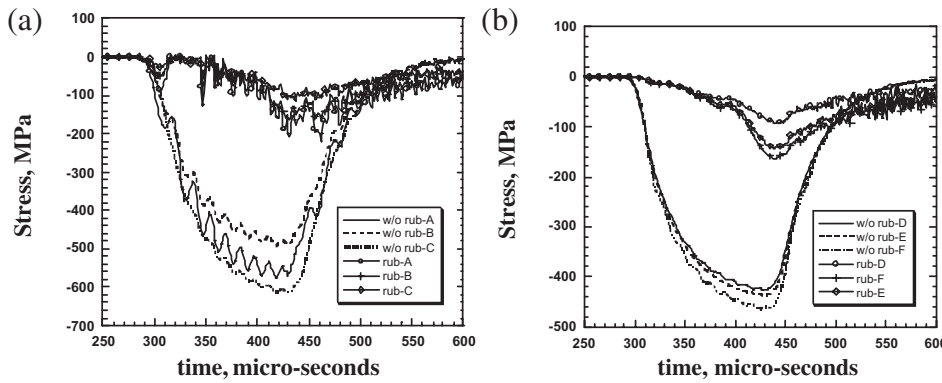

Figure 9. *Comparison of calculated z-stress data at same 3 elements with and without rubber interlayer for (a) ceramic and (b) composite.*

contributes to greatly reduced stress levels within these layers. Also, although the maximum stress is still experienced in each case at about 440 μs, the initial stress build-up for the composite is much delayed and that for the ceramic is the subject of rather complex stress oscillations.

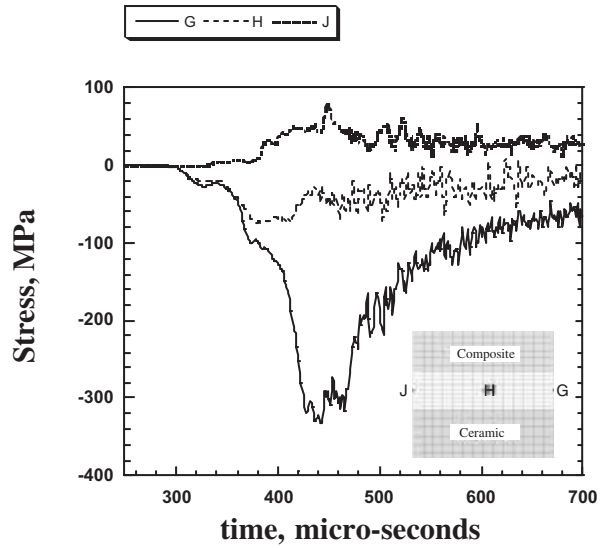

Figure 10. *Compressive stress at midthickness of rubber interlayer for locations at midsection (G), half-radius (H) and surface (J).*

Figure 10 shows the z-stress distributions in the rubber at the midplane level. The centerline z-stress rises slowly for the first $\sim 100\,\mu s$ until the rubber has been significantly compressed and then rises very sharply. Away from the centerline, significant tensile stresses are encountered. Analogous observations are made concerning the in-plane stresses because, again, the (unconstrained) free surface does not allow compressive stresses to be developed there.

DISCUSSION

The motivation for the present work was to understand the dynamic deformation of multilayer composite materials and to validate the initial modeling results. Since the SHPB is a convenient tool for high strain rate testing, this was the test method selected. Direct interpretation of SHPB data is not possible for materials which are nonlinear, or of very low or very high impedance relative to the bars, or anisotropic, or composed of several layers of distinctly different materials. The latter is the case studied here.

Since the experiments have shown that there is excellent agreement between numerical data and actual data measured from the incident and transmitter bars for the two-layer tests, we can conclude that, with some qualifications, the model satisfactorily captures the details of wave transmission. The three-layer model captures the general features of wave propagation and the form of stress distribution but requires further refinement to improve agreement in terms of absolute values of stress.

A unique aspect of this work has been the extensive use of strain gages to generate measured data for comparison with the numerical data. Strain data are converted to stress data assuming a constant value for Young's modulus. Nevertheless, the measured data are generally within a few percent of the numerical data for the single and double layer materials and confirm the validity of the model and of this assumption.

The single layer case has been well documented for metals, ceramics, polymers, composites etc., elsewhere and will not be commented upon further here. The double layer case appears straightforward and, essentially, the response of the ceramic begins to resemble that of the composite [compare Figure 3(a) (or (c)) and Figure 6(a) (or (b)] since the wave propagation is rapidly dominated by the lower impedance composite layer. The presence of the rubber interlayer, on the other hand, introduces major modifications to the wave transmission characteristics.

Consequently, agreement between the two types of data for trilayer material, where the sequences of wave transmission and reflection themselves are much more complex, is currently rather less close, e.g., compare Figure 8(a) and (b) with (c) and (d). Experimental limitations occur since the strain gages average the data over their active gage length, which is typically 0.79 mm as opposed to ~0.4 mm for the element size in the model, and also the measured stress is seen to be very strongly dependent upon the exact placement of the gage within the specimen length.

Bearing these limitations in mind, it can be appreciated that there is nonetheless strikingly good agreement between experimental and numerical data. For example, Figure 8(a) shows experimental data from two gages on the ceramic sample surface, 5 mm apart, and three principal peaks are noted at approximately 60 μs intervals. Also, the magnitude of the stress close to the ceramic–rubber interface is ~0.4 times that at the incident bar–ceramic interface. The numerical data likewise show three major peaks at approximately similar intervals and, interpolating to comparable elemental positions, the relative magnitudes are quite similar. The absolute magnitudes of the maximum measured stresses are, however, somewhat different and this is partially due to reasons of data source location and the "averaging" effect of the strain gage size mentioned previously. The fact that the magnitudes of stresses in the composite in the two- and three-layer materials are greater than the calculated values, also indicates that further refinements in material parameters are necessary.

Due to their finer-scale spatial resolution, the numerical data can provide a clearer picture of the details of wave propagation. Without attempting to give a microsecond by microsecond description, the following can be deduced as the rough sequence of physical events if we remember that the response of each layer is a function of the layer thickness and the material properties of the layer itself as well as the adjacent layers. For our case, rubber is a nonlinear material and its wave velocity is a function of stress–strain amplitude. Therefore, the acoustic impedance and transmission coefficient between the adjacent layers are not constant but are also functions of the stress–strain amplitude [22].

Thus, the first compressive pulse in Figure 8(a) and (b) represents the entry of the compressive stress wave into the ceramic. The elastic wave transit time is ~ 1.4 μs, after which the wave arrives at the ceramic–rubber interface where it is immediately almost completely reflected since the rubber has a very low impedance initially. The reflected tensile wave therefore subtracts from the incoming compressive wave, leading to the low stress plateau seen in Figure 8(b). However, the rubber begins to compress and its impedance rises so that successively more of the wave is transmitted through it and into the composite as shown in Figure 8(d). The following complex sequence of oscillating pulses are due to further reflections from the interfaces between the layers.

It is found that a major effect of rubber is to lead to a highly inhomogeneous stress distribution within the components. The part of the sample close to the rubber experiences a reduced stress while the remainder may experience a much higher stress level, as shown for the ceramic in Figure 9(a). Also, the rapidly fluctuating manner of stress distribution

for the rubber interlayer case will lead to significant local strain gradients and increase the tendency to brittle fracture which is the main failure mechanism for the ceramic. The situation is also similar for the composite. The maximum : minimum stress ratio in the composite, with rubber present, is about 5 and again a fluctuating, nonuniform stress distribution with respect to both time and position can be clearly seen from Figure 9(b). The highly inhomogeneous stress-distribution is, of course, totally different from what is normally assumed to be occurring in SHPB testing after several transit times [23] and graphically underscores the inability of conventional data reduction routines to handle results from these materials.

Figure 10 captures details of the complex history of the rubber layer. While it is compressed between the ceramic and composite, it is expanding in the in-plane direction, causing both in-plane tension and in-plane shear stresses. When a compressive stress pulse propagates through the thickness of the rubber, a highly compressive state of stress is developed in center of the rubber layer due to the constraining effect of the ceramic–rubber and rubber–composite interfaces. Closer to the surface, the stress rises less before decreasing and at the surface it even becomes tensile. The rubber also expands in the in-plane direction towards the traction-free surface with an accompanying increase in the x-stress. The x-stress is greatest at the centerline of the sample and decreases toward the free surface, again becoming tensile there in the same manner as the z-stress. Similar behavior of EPDM rubber subjected to compressive stress wave loading has been reported by Gama et al. [22].

Several final comments are also in order concerning future developments of the model and the relevance of the present tests to actual bulk applications. Samples used in this work were, at the most, 15 mm in diameter and considerable radial strain was noted in the composites indicating the existence of radial stresses. Larger samples, typical of many anticipated applications, would be subjected to severe lateral constraints which would in turn affect the through thickness stresses reported here. Also, it should be noted that the samples are subjected to an essentially rigid backing (the transmitter bar), whereas significant elastic bending deflection would be encountered in a real, unsupported composite plate. Since it has been reported that the ratio of energy absorbed by elastic deflection to that absorbed by local indentation is strongly dependent upon sample thickness [12,13], future work will be directed towards allowing deflection of the backing plate.

Further work is already underway to investigate experimentally and numerically the effects of lateral confinement of the rubber interlayer. The numerical model is also being modified so as to incorporate the viscoelastic effects, cumulative damage in the composite. Also it is clear that a realistic model for the nature of the rubber–ceramic and rubber–composite interfaces is vital to achieve good agreement between experiment and calculations. The effects of sliding and/or friction at the rubber–composite and rubber–ceramic interfaces will be incorporated, based on careful observations of actual tested samples.

CONCLUSIONS

LS-DYNA has been successfully used to model the results of SHPB tests on multilayer composite materials. Strain gage data has been used to validate the models. For the present materials, whether the higher impedance layer was placed in front of the lower

impedance layer or vice versa, little influence was observed on the wave propagation characteristics within the latter. However, the introduction of an unconstrained rubber interlayer between the two major structural layers led to a reduction of the maximum stress level in each layer as well as highly inhomogeneous and rapidly varying stress distributions within each layer.

ACKNOWLEDGMENT

The authors gratefully acknowledge financial support for this research under Composite Materials Research (CMR) Collaborative Program sponsored by the Army Research Laboratory, contract number DAAD19-01-2-0001.

REFERENCES

1. Zhao, H. and Gary, G. (1997). An Experimental Investigation of Compressive Failure Strength of Fibre-reinforced Polymer-matrix Composite Plates Under Impact Loading, *Composites Science and Technology*, **57**(3): 287–292.
2. Lopatnikov, S.L. et al. (2003). Dynamics of Metal Foam Deformation During Taylor Cylinder-Hopkinson Bar Impact Experiment, *Composite Structures*, **61**(1–2): 61–71.
3. Lopatnikov, S.L. et al. High-velocity Plate Impact of Metal Foams, *International Journal of Impact Engineering*, In Press.
4. Lee, S.W.R. and Sun, C.T. (1993). Dynamic Penetration of Graphite-Epoxy Laminates Impacted by a Blunt-Ended Projectile, *Composites Science and Technology*, **49**(4): 369–380.
5. Goldsmith, W., Dharan, C.K.H. and Chang, H. (1995). Quasi-Static and Ballistic Perforation of Carbon-Fiber Laminates, *International Journal of Solids and Structures*, **32**(1): 89–103.
6. Wu, E.B., Tsai, C.Z. and Chen, Y.C. (1994). Penetration into Glass Epoxy Composite Laminates, *Journal of Composite Materials*, **28**(18): 1783–1802.
7. Abrate, S. (2001). Modeling of Impact on Composite Structures, *Comp. Struct.*, **51**: 129–138.
8. Collombet, F. et al. (1998). Damage Criteria for the Study of Impacted Composite Laminates, *Composites Science and Technology*, **58**(5): 679–686.
9. Chen, J.K., Allahdadi, F.A. and Carney, T.C. (1997). High-velocity impact of graphite/epoxy composite laminates, *Composites Science and Technology*, **57**(9–10): 1369–1379.
10. DeLuca, E. et al. (1998). Ballistic Impact Damage of S-2-glass-Reinforced Plastic Structural Armor, *Composites Science and Technology*, **58**(9): 1453–1461.
11. Gama, B.A. et al. (2001). High Strain-rate Behavior of Plain-weave S-2 Glass/vinyl Ester Composites, *Journal of Composite Materials*, **35**(13): 1201–1228.
12. Kim, J.K. and Kang, K.W. (2001). An Analysis of Impact Force in Plain-weave Glass/Epoxy Composite Plates Subjected to Transverse Impact, *Composites Science and Technology*, **61**(1): 135–143.
13. Cantwell, W.J. and Morton, J. (1989). Geometrical Effects in the Low Velocity Impact Response of CFRP, *Composite Structures*, **12**(1): 39–59.
14. Mines, R.A.W., Roach, A.M. and Jones, N. (1999). High Velocity Perforation Behaviour of Polymer Composite Laminates, *International Journal of Impact Engineering*, **22**(6): 561–588.
15. Wen, H.M. (2001). Penetration and Perforation of Thick FRP Laminates, *Composites Science and Technology*, **61**(8): 1163–1172.
16. Nayfeh, A.H. (1991). The General Problem of Elastic Wave-Propagation in Multilayered Anisotropic Media, *Journal of the Acoustical Society of America*, **89**(4): 1521–1531.
17. Fink, B.K. (2000). Performance Metrics for Composite Integral Armor, *Journal of Thermoplastic Composite Materials*, **13**(5): 417–431.

18. Gama, B.A., Gillespie, J.W. Jr., Mahfuz, H., Bogetti, T.A. and Fink, B. (2000). Effect of Non-Linear Material Behavior on the Through-Thickness Stress Wave Propagation in Multi-Layer Hybrid Lightweight Armor, *Advances in Comp*, *Eng. and Sci*., Tech. Sci. Press.
19. Gama, B.A., Gillespie, J.W. Jr., Bogetti, T.A. and Fink, B. (2001). Innovative Design and Ballistic Performance of Lightweight Composite Integral Armor, *SAE 2001 World Congress*, Detroit, SAE, MI.
20. Mahfuz, H. et al. (2000). Investigation of High-velocity Impact on Integral Armor using Finite Element Method, *International Journal of Impact Engineering*, **24**(2): 203–217.
21. Guden, M. and Hall, I.W. (1998). Dynamic properties of Metal Matrix Composites: A Comparative Study, *Materials Science and Engineering A: Structural Material Properties Microstructure and Processing*, **242**(1–2): 141–152.
22. Gama, B.A., Bogetti, T. A., Fink, B., Mahfuz, K. and Gillespie, J.W. Jr. (1999). Modeling and Simulation of the Dynamic Behavior of EPDM Rubber under Stress Wave Loading, In: *Proc. Conf*. "*Math. & Computers in Mech. Eng*. '*99*", Florida.
23. Ravichandran, G. and Subhash, G. (1994). Critical-Appraisal of Limiting Strain Rates for Compression Testing of Ceramics in a Split Hopkinson Pressure Bar, *Journal of the American Ceramic Society*, **77**(1): 263–267.